On reformation of quasi-perpendicular collisionless shocks

Matsukiyo, Shuichi
Department of Earth System Science and Technology, Kyushu University | Max-Planck-Institut für extraterrestrische Physik

Scholer, Manfred
Max-Planck-Institut für extraterrestrische Physik | Department of Earth System Science and Technology, Kyushu University

出版情報：Advances in Space Research. 38, pp.57-63, 2006. Elsevier
バージョン：

REFORMATION OF QUASI-PERPENDICULAR SHOCKS WITH REALISTIC ION TO ELECTRON MASS RATIO

S. Matsukiyo and M. Scholer[1]

[1] *Centre for Interdisciplinary Plasma Science, Max-Planck-Institut fur extraterrestrische Physik, 85741, Garching, Germany*

ABSTRACT

Mass ratio dependence of self-reformation of high Mach number quasi-perpendicular shock waves is investigated by means of one-dimensional full particle simulation code. In small ion to electron mass ratio runs, the reformation is due to the accumulation of gyrating reflected ions. Furthermore, at the extremely small mass ratio, the Buneman instability is generated in the foot. In the realistic mass ratio run, however, the modified two-stream instability excited in the foot leads to the reformation.

INTRODUCTION

Reformation of quasi-perpendicular shocks has been investigated by a number of authors (Biskamp and Welter, 1972; Leroy, 1983; Lembege and Dawson, 1987; Lembege and Savoini, 1992). In high Mach number shocks, some of the incoming ions are reflected at the ramp, and they form the foot in front of the ramp during their gyration. At the upstream edge of the foot, they are accumulated in time and are responsible for the reformation. Therefore, it has been recognized that the reformation inseparably relates to ion dynamics. In addition, recent full particle simulations show the importance of electron dynamics in the foot. Shimada and Hoshino (2000) studies the Buneman instability in the foot of a perpendicular shock and resulting electron hole formation. Schmitz et al. (2002) and Shimada and Hoshino (2004) discuss the wave-particle interactions in the foot in more detail.

However, most of the past full particle simulations assume unrealistically small ion to electron mass ratios. Recently, Scholer et al. (2003) confirmed by performing one-dimensional full particle simulations of quasi-perpendicular shocks that the reformation occurs at realistic mass ratio too if the ion beta is low ($\beta_i = 0.2$). Furthermore, they observed the modified two-stream (MTS) instability in the foot instead of the Buneman instability seen in a small mass ratio run.

In this study, we perform three full particle simulations with different mass ratios in order to investigate the mass ratio dependence of structure of high Mach number quasi-perpendicular shocks and of wave-particle interactions in the transition region. In the next section the simulation results are represented, and the following section analyzes the instabilities observed in the foot. Finally, the results are summarized and discussed.

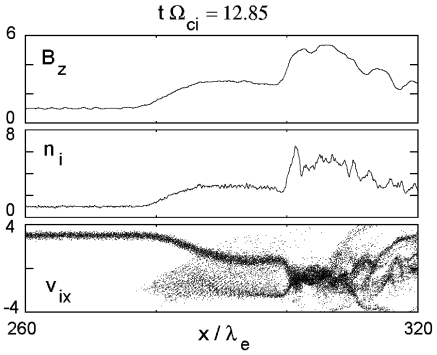

Fig. 1. From top to bottom: magnetic field B_z component, ion density n_i, and ion v_{ix} phase space versus shock normal direction x for run 1 ($\mu = 80$).

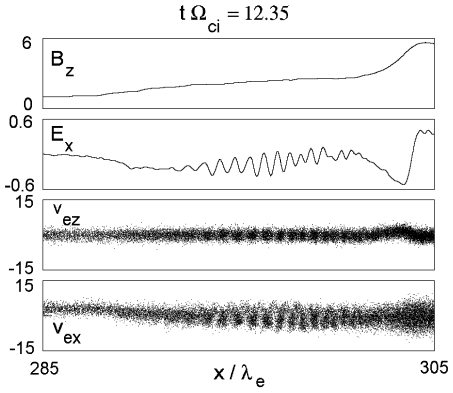

Fig. 2. From top to bottom: magnetic field B_z component, electric field component E_x, and electron v_{ez} phase space versus shock normal direction x for run 1.

NUMERICAL SIMULATIONS

We present here the simulation results for three different values of ion to electron mass ratio (μ) while all other parameters are the same. A one-dimensional electromagnetic full particle code is utilized. The system is initialized by injecting a uniform plasma composed of electrons and ions from the left hand boundary at $x = 0$ where the plasma carries a uniform magnetic field polarized in $x - z$ plane. The plasma is continuously injected and travels toward the $+x$ direction, and is specularly eflected at the right hand baundary. Then a shock is produced and propagates in the $-x$ direction so that the simulation system is the downstream rest frame.

The physical parameters used in the simulation runs are as follows. The injection Alfvén Mach number is $M_{A0} = 3.0$ which leads to a $M_A \sim 4.5$ shock. The upstream ion and electron beta are $\beta_i = \beta_e = 0.05$. The angle between the uniform magnetic field and a shock normal (x) direction is $\Theta_{Bn} = 87°$. Because of computational restrictions the squared ratio of the upstream electron plasma to cyclotron frequencies ($\tau \equiv \omega_{pe}^2/\Omega_e^2$) is set to 4. The technical parameters are represented by Scholer and Matsukiyo (2004). In the following, we present simulation results for three different values of μ.

RUN 1 : $\mu = 80$

Figure 1 shows a typical example of a supercritical quasi-perpendicular shock profile. From top to bottom, the magnetic field B_z component, the ion density n_i, and the ion $v_{ix} - x$ phase space plot at $\Omega_{ci}t = 12.85$ are represented, where Ω_{ci} denotes the ion cyclotron frequency. Some of the incoming ions are specularly reflected at the ramp ($x/\lambda_e \sim 300$), and they form a well developed foot in front of the ramp, where λ_e denotes the electron enertial length. In a later stage they accumulate at the edge of the foot due to their gyration with accompnied by further deceleration of the incoming ions which results in a reformation.

Furthermore, it is seen in Figure 2 that the Buneman instability is generated in the foot. The electrostatic wave component, E_x, is dominantly amplified. Accordingly, the electrons are heated mainly in v_{ex} which is almost perpendicular to the static magnetic field. The waves propagate in the $-x$ direction so that the instability is due to the interaction between the electrons and the reflected

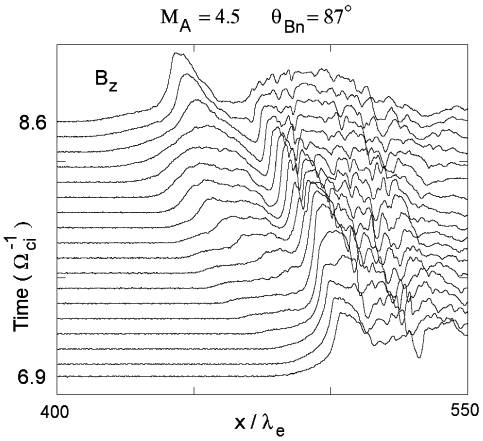

Fig. 3. Magnetic field B_z component stacked in time for run 2 ($\mu = 400$). Time runs from bottom to top.

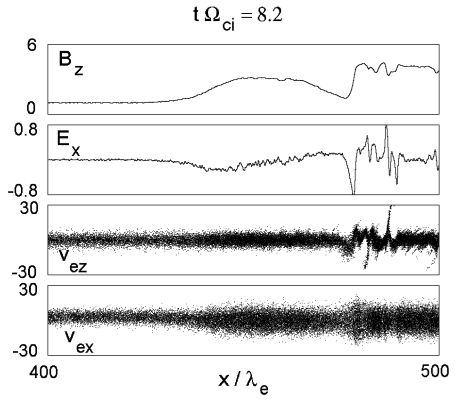

Fig. 4. The same format as Figure 2 for run 2.

ions. This type of the instability and the associated wave-particle interactions is well discussed by Shimada and Hoshino (2000; 2004) and Schmitz et al. (2002).

RUN 2 : $\mu = 400$

In this case too, the simulation shows a typical reformation cycle seen in Figure 3 which represents a stacked plot of magnetic field B_z component during the time period of $6.9 \leq \Omega_{ci}t \leq 8.6$. At $\Omega_{ci}t = 6.9$ the ramp is located at $x/\lambda_e \sim 500$. As time has past the clear foot structure is gradually developed in front of the ramp, and finally the new ramp appears at it's upstream edge ($x/\lambda_e \sim 440$). The same process is observed also in run 1 although it is not shown here.

However, the Buneman instability in the foot is not found in this case. Two field components (B_z and E_x) do not show wavy structures, and the electrons are just adiabatically heated in perpendicular velocity space (v_{ex}) in Figure 4 which is the same format as Figure 2. This is because the instability is Landau damped as discussed later.

RUN 3 : $\mu = 1840$

In the realistic mass ratio case a reformation again occurs, but the characteristics are different from the previous cases, run 1 and run 2. Figure 5 again indicates one reformation cycle with the same format as Figure 3. A sharp ramp appears both at the beginning of the cycle ($\Omega_{ci}t = 3.0$) and at the end ($\Omega_{ci}t = 4.8$). In between, however, the field is strongly fluctuated in the transition region and even the ramp is not clearly recognized. Figure 6 shows the B_z, n_i, and v_{ix} phase space versus x at $\Omega_{ci}t = 4.5$ in the same format as Figure 1. In the region where the field is turbulent, the reflected and the incoming ions are phase mixed and cannot be separated anymore in contrast to the small mass ratio runs (cf. Figure 1). After the two ion components are sufficiently phase mixed, the new ramp appears at the edge of the turbulent region. This turbulent field is generated by the modified two-stream (MTS) instability which is analyzed in the next section.

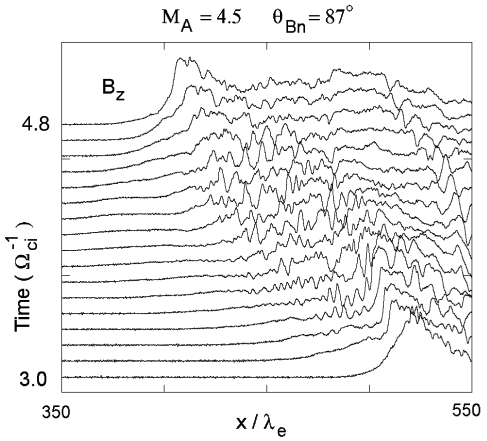

Fig. 5. Magnetic field B_z component stacked in time for run 3 ($\mu = 1840$). Time runs from bottom to top.

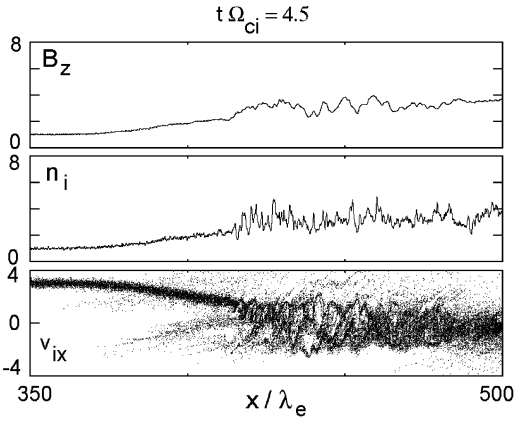

Fig. 6. The same format as Figure 1 for run 3.

INSTABILITIES IN THE FOOT

One of the important features in a high Mach number quasi-perpendicular shock is wave excitation in the foot. Because of the presence of reflected ions, bulk velocity of ions in the foot decreases. Then, electron bulk velocity should also decrease in the foot by requiring zero current in the shock normal direction. As a result, a finite difference of the bulk velocities between the electrons and the incoming/reflected ions arises. Such a velocity difference can lead to some instabilities.

When we pay attention to the waves which have frequencies much higher than the ion cyclotron frequency and wave lengths much smaller than the ion gyroradius as seen in our simulation runs, ions are assumed to be unmagnetized and two instabilities are possibly generated. One is the Buneman instability which is based on the interaction between the reflected/incoming ion beam and the Landmuir wave. Another one is the MTS instability which is due to the interaction between the incoming/reflected ion beam and the oblique whistler wave. Because we assume $\beta_i = \beta_e$ in the simulations, the ion acoustic instability is not generated. The dispersion relation of a cold plasma which is consist of an electron and one ion component is described as

$$\left(1 - \frac{\omega_{pi}^2}{(\omega - ku_i)^2} - \frac{\omega_{pe}^2}{\omega^2}\right)\left(1 - \frac{\Omega_{ce}^2 \cos^2\Theta_{Bn}}{\omega^2(1+H_e)^2}\right) - \frac{\Omega_{ce}^2 \sin^2\Theta_{Bn}}{\omega^2(1+H_e)}\left(1 - \frac{\omega_{pi}^2}{(\omega - ku_i)^2}\right) = 0, \quad (1)$$

where ω_{pi}, ω_{pe}, and Ω_{ce} denote the ion, electron plasma, and the electron cyclotron frequencies, $H_e = 1/k^2\lambda_e^2$, respectively. The relative ion beam velocity to the electrons is indicated by u_i so that our calculations are done in the electron rest frame. The assumptions adopted in deriving eq. (1) are summarised by Matsukiyo and Scholer (2003). Eq. (1) indicates that the electrostatic and the electromagnetic oscillations are decoupled when $\Theta_{Bn} = 0$. In this case the ion beam can generate only the electrostatic plasma oscillation through the Buneman instability, while the electromagnetic whistler wave is stable. However, if Θ_{Bn} is finite, the ion beam can interact also with the whistler waves, and this is the modified two-stream instability. Figure 7 shows the solution of eq. (1) for $\mu = 100, \Theta_{Bn} = 60°, \tau = 4$, and $u_i/v_A = 1$. The real (upper panel) and the imaginary (lower panel) parts of the frequency are shown as a function of the wavenumber. Both of the Buneman and the

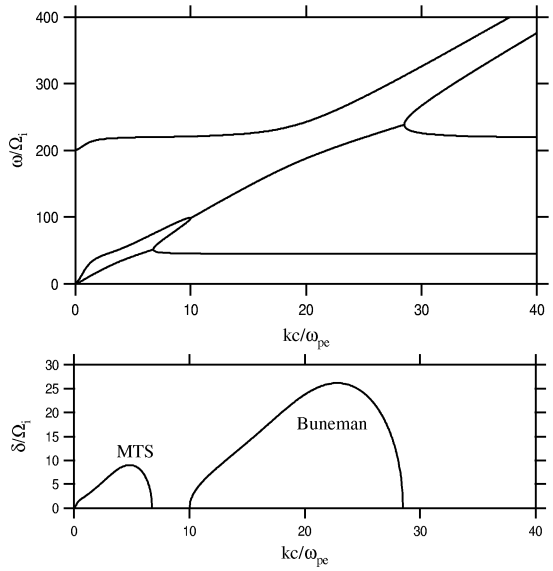

Fig. 7. Dispersion relation in the cold plasma limit.

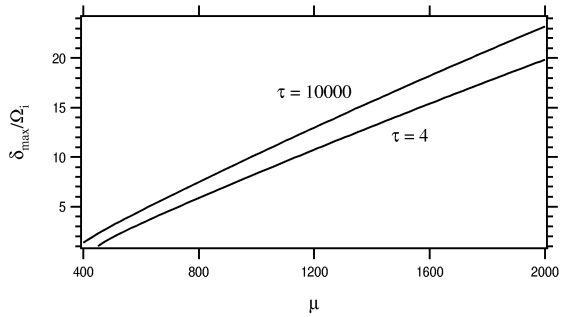

Fig. 8. Mass ratio dependence of the maximum growth rate of the modified two-stream instability.

MTS instabilities have positive growth rates. One should note that the instability is stabilized at $\Theta_{Bn} = 90^\circ$ bacause the term proportional to $\cos^2\Theta_{Bn}$ in eq. (1) vanishes.

BUNEMAN INSTABILITY

The Buneman instability is a strong instability in a cold plasma. However, it is known that the growth of this instability is strongly supressed by the Landau damping when the relative drift velocity between electrons and reflected ions are of the same order of or smaller than the electron thermal velocity. The above condition is written as $\beta_e \gtrsim 4M_A^2/\mu(1+\alpha)^2$ if the current conservation in the foot is assumed, where α denotes the density ratio of reflected to incoming ions. This is the condition satisfied in case of parallel propagation, i.e., $\Theta_{Bn} = 0$. However, it is also true for an arbitrary propagation angle if $\omega_{pe} > \Omega_{ce}$ since the wave frequency is greater than Ω_{ce} in such a case, i.e., electrons are effectively unmagnetized. When we assume $\mu = 1840$ and $\alpha = 0.25$, the Buneman instability cannot grow unless $\beta_e \ll M_A^2/720$. For the Earth's bow shock ($M_A \sim 5$) $\beta_e \ll 0.035$ is required, although it is a rare case. One should note that this upper limit of β_e for the Buneman instability increases if unrealistically small μ is assumed. Therefore, effects of the Buneman instability are overestimated in small μ runs.

In run 1 ($\mu = 80$) the upper limit of β_e is 0.65 which is much lager than the actual value of $\beta_e = 0.05$. Therefore the instability is clearly seen in Figure 2. In run 2 ($\mu = 400$), on the other hand, the upper limit of β_e is estimated as 0.13. It is still larger than 0.05, but the instability is not observed in Figure 4. This is explained as follows. The above estimation of the upper limit of β_e is based on the current conservation in the foot by using the injection velocity as the incoming ion bulk velocity. However, the incoming ions are actually pre-decelerated in the foot so that the actual upper limit of β_e should be smaller than 0.13. In run 2 the relative bulk velocity of the incoming ions to the electrons in the foot is about half of the injection velocity. It means the upper limit of β_e is ~ 0.03 which is smaller than 0.05. This is the reason why the instability is stabilized. It is clear now that the Buneman instability is not observed in run 3 ($\mu = 1840$) too.

MODIFIED TWO-STREAM INSTABILITY

As mentioned earlier in this section, the MTS instability is based on the interaction between a cross field ion beam and an oblique whistler wave. Hence, the instability is stabilized when the ion beam cannot interact with the whistler waves, i.e., when u_i exceeds the maximum phase velocity of whistler wave which is described as $\omega/kv_A \approx (\mu^{1/2}\cos\Theta_{Bn})/2$ for $\tau \gg 1$. From the zero current condition in the foot, $|u_i|/v_A = 2M_A/(1+\alpha)$ for reflected ions while $|u_i|/v_A = 2\alpha M_A/(1+\alpha)$ for incoming ions. As a result, the instability get excited if $\cos\Theta_{Bn} > 4M_A/\mu^{1/2}(1+\alpha)$ by the electron-reflected ion interaction, and if $\cos\Theta_{Bn} > 4\alpha M_A/\mu^{1/2}(1+\alpha)$ by the electron-incoming ion interaction, respectively. Since $\alpha < 1$, the instability of the latter type can be destabilized in a wider range of Θ_{Bn} compared with the instability of the former type.

Figure 8 represents the maximum growth rate normalized to ion cyclotron frequency, δ_{max}/Ω_{ci}, of the MTS instability through the electron-incoming ion interaction versus μ for $u_i/v_A = 1.8$, $\Theta_{Bn} = 87^\circ$, and $\tau = 4$ and 10^4 , where v_A is the upstream Alfvén velocity. It is seen that δ_{max}/Ω_{ci} increases with μ but do not depend on τ so much. As a result, if the mass ratio is realistic ($\mu = 1840$), the growth rate is much larger than the ion cyclotron frequency which characterizes the shock reformation cycle. In other words, unrealistically small μ may prevent the instability in the foot within a reformation cycle regardless of the value of τ. This is the reason why the MTS instability is not observed in run 1 and run 2.

However, in run 3 we can see the instability in the foot. Figure 9 shows from top to bottom the magnetic field B_z, the electric field E_x, and electron v_{ez} and ion v_{ix} phase space versus x in the foot of the shock at $\Omega_{ci}t = 3.7$ in run 3. Both of the B_z and E_x field components show the wavy structure, and they are correlated each other. Furthermore, the electrons are trapped in v_{ez} by the wave while the incoming ions are trapped in v_{ix}. The reflected ions are not directly affected by the wave in this stage. The above characteristics are clearly those of the MTS instability through the electron-incoming ion interaction as shown by Matsukiyo and Scholer (2003) and Scholer et al. (2003). The above condition of the instability is satisfied only for the electron-incoming ion interaction by taking the pre-deceleration of the incoming ions in the foot into account. In the MTS instability ions are almost unmagnetized while electrons are strongly magnetized since the generated wave frequency is between the ion and the electron cyclotron frequencies. The main electric field is parallel to the shock normal ($x-$direction) so that the ions are trapped in v_{ix} by this E_x field. However, the magnetized electrons cannot move in the $x-$direction across the magnetic field. Instead, they feel the parallel electric field of the obliquely propagating wave, and are trapped by the paralled electric field which is almost parallel to the $z-$direction. In the later stage at $\Omega_{ci}t = 4.5$, the wave amplitude sufficiently increases and both of the incoming and reflected ions are thermalized as seen in Figure 6. When the most of the reflected ions are thermalized, the new shock ramp appears at $\Omega_{ci}t = 4.8$ in Figure 5.

We should discuss here the kinetic effects of the MTS instability. According to Matsukiyo and Scholer (2003), the main kinetic effect in the MTS instability is the electron Landau damping. The electron Landau damping in the Buneman instability is strong when $\omega/k \sim u_i \lesssim v_{the}$ as mentioned already, although that of the MTS instability is strong when $\omega/k_\parallel \sim u_i/\cos\Theta_{Bn} \lesssim v_{the}$ because the electrons are magnetized, where v_{the} denotes the electron thermal velocity. The latter condition is written as $\beta_e \gtrsim 4\alpha^2 M_A^2/[\mu(1+\alpha)^2\cos^2\Theta_{Bn}]$ for the electron-incoming ion interaction. Therefore the MTS instability can survive for larger values of β_e compared with the Buneman instability.

SUMMARY AND DISCUSSIONS

We performed three full particle simulations of quasi-perpendicular shocks with different ion to electron mass ratios, μ, while other parameters ($M_{A0}, \beta_i, \beta_e, \tau$, and Θ_{Bn}) are unchanged. In the low β_i plasma

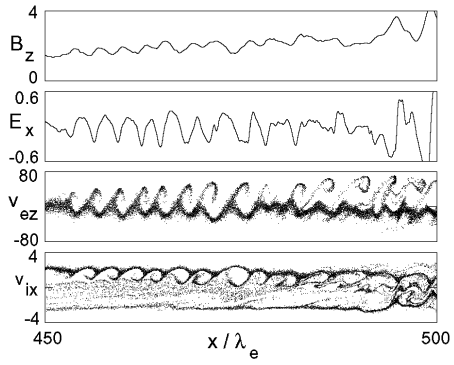

Fig. 9. From top to bottom: magnetic field B_z component, electric field E_x component, electron v_{ez} phase space distribution and ion v_{ix} phase space distribution in the foot of the shock at $\Omega_{ci}t = 3.7$ in run 3.

treated here reformation processes are observed in all the three runs, although it is shown by Scholer et al. (2003) that a shock is stational at higher $\beta_i (> 0.4)$. In the two unrealistically small μ runs, the reformation is due to the accumulation of the gyrating reflected ions at the upstream edge of the foot. Furthermore, at the smallest mass ratio ($\mu = 80$), the Buneman instability is generated leading to the electron heating parallel to the shock normal since the electron thermal velocity is artificially smaller than the relative bulk velocity between electrons and reflected ions. On the other hand, at the realistic mass ratio, the MTS instability which is suppressed in the small μ runs gets excited in the foot due to the electron-incoming ion interaction leading to the electron heating parallel to the magnetic field. When the instability grows enough both of the incoming and the reflected ions are phase mixed and the new shock ramp appears at the upstream edge of the foot.

Since the reformations occur within $1 \sim 2\Omega_{ci}^{-1}$ for all three runs, it is difficult to separate the reformation due to the MTS instability from that due to the gyration of reflected ions. These two processes may simultaneously work in run 3. Therefore, we performed an additional run assuming the same parameters as run 3 except for $\Theta_{Bn} = 90^\circ$. In this case the MTS instability does not take place as mentioned already so that the reformation must be purely due to the accumulation of gyrating reflected ions. Figure 10 shows $v_{ix} - x$ phase space plots at two different times $\Omega_{ci}t = 4.5$ and 5.0. The solid lines indicate the magnetic field profiles at corresponding times. In the top panel the reflected ions just start gyrating back at the edge of the foot. After that, the incoming ions as well as the reflected ions are further accumulated at the edge of the foot and the new ramp appears as seen in the bottom panel. At this time the reflected ions are strongly thermalized and penetrate downstream. In addition, a big ion hole is produced at $x/\lambda_e \sim 420$ as a remnant of this process. In contrast to this run, run 3 represents different properties of the reformation. Figure 11 again shows $v_{ix} - x$ phase space plots at $\Omega_{ci}t = 4.1$ and 4.6 for run 3. The MTS instbility produces highly turbulent field at $\Omega_{ci}t = 4.1$, while vely few parts of the reflected ions start gyrating back at the edge of the foot. At $\Omega_{ci}t = 4.6$, the incoming and most of the reflected ions are phase mixed by the instability without clear signature of the gyrating back ion population. Furthermore, the reformation time scale ($\sim 1.6\Omega_{ci}^{-1}$) in run 3 is shorter than that ($\sim 2.1\Omega_{ci}^{-1}$) obtained in the run assuming $\Theta_{Bn} = 90^\circ$. Hence, the MTS instability may play a dominant role in the reformation process in run 3.

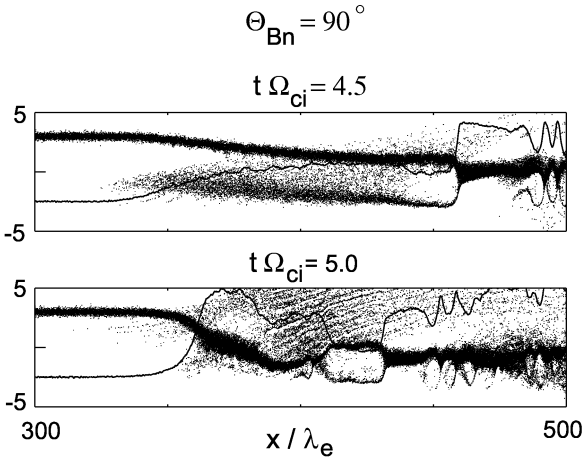

Fig. 10. Ion $v_{ix}-x$ phase space plots at $\Omega_{ci}t = 4.5$ (top panel) and $\Omega_{ci}t = 5.0$ (bottom panel) for the realistic mass ratio run with $\Theta_{Bn} = 90°$. The solid lines denote the profile of the magnetic field B_z component.

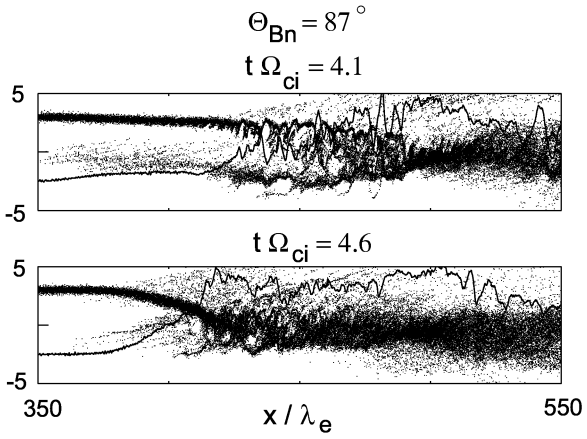

Fig. 11. Ion $v_{ix}-x$ phase space plots at $\Omega_{ci}t = 4.1$ (top panel) and $\Omega_{ci}t = 4.6$ (bottom panel) for run 3. The solid lines denote the profile of the magnetic field B_z component.

Our simulations are performed only for almost perpendicular shocks ($\Theta_{Bn} = 87°$) in order to exclude standing whistler waves which is allowed to exist if $M_A < \mu^{1/2}(\cos\Theta_{Bn}/2)$ (Kennel et al., 1985; Krasnoselskikh et al., 2002). However, the standing whistler waves can also play important roles in more oblique shocks. We will investigate in the future behaviour of shocks when both of the MTS instability and the standing whistler waves are simultaneously present.

ACKNOWLEDGEMENTS

We are grateful to D. Biskamp, B. Lembege, and R. A. Treumann for usefull discussions. The numerical code was provided by I. Shinohara.

REFERENCES

Biskamp, D. and H. Welter, Numerical studies of magnetosonic collisionless shock waves, *Nuclear Fusion*, **12**, 663–666, 1972.

Kennel, C., J. P. Edmiston, and T. Hada, in *Collisionless shocks in the heliosphere: A tutorial review* , Edt. R. G. Stone and B .T .Tsurutani, Geophys. Monographs **34**, American Geophys. Union, Washington, D. C., 1–36, 1985.

Krasnoselsskikh, V. V., B. Lembege, P. Savoini, and V. V. Lobzin, Nonstationarity of strong collisionless quasiperpendicular shocks: Theory and full particle simulations, *Phys. Plasmas*, **9**, 1192–1209, 2002.

Lembege, B. and J .M .Dawson, Self-consistent study of a perpendicular collisionless and nonresistive shock, *Phys. Fluids*, **30**, 1767–1788, 1987.

Lembege, B. and P .Savoini, Non-stationarity of a two-dimensional quasi-perpendicular supercritical collisionless shock by self-reformation, *Phys. Fluids B*, **4**, 3533–3548, 1992.

Leroy, M. M., Structure of perpendicular shocks in collisionless plasma, *Phys. Fluids*, **26**, 2742–2753, 1983.

Matsukiyo, S. and M. Scholer, Modified two-stream instability in the foot of high Mach number quasi-perpendicular shocks, *J. Geophys. Res.*, **108**, 1459,doi:10.1029/2003JA10080, 2003.

Schmitz, H., S. C. Chapman, and R. O. Dendy, Electron preacceleration mechanisms, in the foot region of high Alfvénic Mach number shocks, *Astrophys. J.*, **579**, 327–336, 2002.

Scholer, M., I. Shinohara and S. Matsukiyo, Quasi-perpendicular shocks: Length scale of the cross-shock potential, shock reformation, and implication for shock surfing, *J. Geophys. Res.*, **108**, 1014,doi:10.1029/2002JA009515, 2003.

Scholer, M. and S. Matsukiyo, Nonstationarity of quasi-perpendicular shocks: Full particle simulation with realistic ion to electron mass ratio, *Annales Geophysae*, in press, 2004.

Shimada, N. and M. Hoshino, Strong electron acceleration at high Mach number shock waves: Simulation study of electron dynamics, *Astrophys. J. Lett.*, **543**, L67–L71, 2000.

Shimada, N. and M. Hoshino, Electron heating and acceleration in the shock transition region: Background plasma parameter dependence, *Phys. Plasmas*, **11**, 1840–1849, 2004.